Design and Test of a Small-Scale, Additively-Manufactured, Liquid-Cooled Rocket Nozzle

Matthew R. Durkee[1], Connor A. McCain[1], Andrew J. Quinton[2], Kathryn A. Stewart[1],
Lucas Utley[1], and Kurt P. Rouser[3]
Oklahoma State University, Stillwater, OK, 74078-5016

The purpose of this study is to design and test additively manufactured rocket nozzles that incorporate liquid cooling during a solid propellant motor burn to evaluate the feasibility of small-scale regenerative cooling in terms of reusability, cost, and reduced manufacturing time. Tests are meant to replicate high pressure, temperature, and mass flux conditions similar to small liquid rocket engines as used in SmallSat and RCS thrusters. Liquid cooling is typically used in rocket nozzles to ensure the inner wall temperature is below the material melting or deformation point, despite exhaust gases exceeding those temperatures. Additively-manufactured nozzles are particularly useful for liquid cooling because complex internal passages may be integrated within the printed part. The nozzles in this study were designed to fit inside a 1.5-inch diameter motor casing and tested on a static thrust stand capable of measuring 500 pounds of thrust. Experiments were conducted using potassium nitrate-sorbitol (KNSB) solid rocket motors to produce high pressure, hot exhaust gas conditions. Nozzle test articles included 3D-printed plastic nozzles made of Polylactic Acid (PLA) and nylon Selective Laser Sintering (SLS). Results include hotfires that featured reduced nozzle throat erosion with cooling flows of 4.59in^3/s of water at 70°F. An uncooled nozzle of identical materials and dimensions melted and widened the throat 370% due to high temperatures and exhaust mass flux, whereas a cooled nozzle's throat diameter increased 225%. These high percentages are likely attributed to the use of polymers, but more thermally-resilient yet affordable materials, metals such as aluminum or steel in particular, suggest potential for this application. An analytical study is performed to further explain the experimental observations. Use of liquid cooling and additive manufacturing shows favorable potential for increased reusability, lower cost, shorter manufacturing time and decreased material usage in small-scale rocket nozzles.

Nomenclature

A	=	area, ft^2
$\dot{m}$	=	mass flow rate, kg/s
P	=	pressure, Pa
V_{avg}	=	average velocity, ft/s
$\dot{V}$	=	volumetric flow rate, L/hr
ρ	=	density, kg/L

I. Introduction

REGENERATIVE cooling is a thermal management method for many liquid propellant rocket engines in which a liquid propellant is circulated through passages in the rocket nozzle to remove heat and prevent hardware thermal damage. Other thermal management techniques exist including film cooling, ablation, and radiation cooling that use propellant or exhaust gases for cooling not combustion (film cooling), erode the nozzle geometry (ablation), or rely on advanced materials to remove heat (radiation). Regenerative cooling is advantageous because the same propellant used for cooling is put towards combustion. Additionally, it preheats the propellant and augments the

[1] Graduate Student, Mechanical and Aerospace Engineering, 201 General Academic Building, Student Member
[2] Undergraduate Student, Mechanical and Aerospace Engineering, 201 General Academic Building, Student Member
[3] Assistant Professor, Mechanical and Aerospace Engineering, 201 General Academic Building, Associate Fellow

initial energy content of the propellant prior to combustion.[1] The cooling passages generally consist of numerous small tubes that are formed into special shapes and contours and then brazed or welded together[2] by traditional manufacturing techniques, as seen below in Fig. 1. This is suitable for medium to large-scale rocket engines;[3] however, these coolant passages can be complex and costly to manufacture. It is for this reason that regenerative cooling has seen little application to smaller sized nozzles. However, the advent of additive manufacturing (AM) opens potential for regenerative cooling to be used on smaller-scale propulsion systems where traditional manufacturing of these passages may have been impractical or unnecessary. Small-scale rocket nozzles (4-inch outer diameter or less) are in the realm of many reaction control system or SmallSat thrusters and may benefit from advances in liquid cooling of nozzles. Nozzles may now be printed in a single piece with complex internal and external geometries for cooling channels, curves, fittings and attachments.

The goal of the current study is to use AM to create a water-cooled nozzle for use on small-scale solid propellant rocket motors that simulate hot (up to 2400°F), high-pressure (up to 1000 PSI) exhaust gases present in liquid propellant systems. Specific objectives include: 1) evaluate the feasibility of additively manufacturing a small, cooled nozzle, 2) experimentally analyze nozzle ablation with the addition of cooling and 3) explain melting and damage experienced in experiments using computational fluid dynamics (CFD).

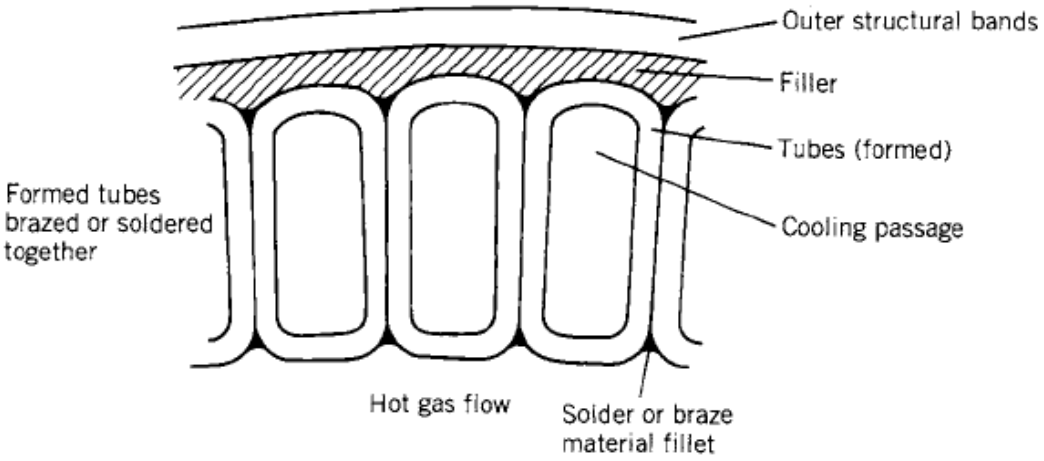

Figure 1: Cross Section of a Traditionally-Manufactured Cooling Jacket[4]

II. Background

A. Theory

In order to provide the boundary conditions for the computational model and have values to compare between the experimental nozzle exit properties and those calculated by the computational model, the nozzle inlet and exit velocity and pressure had to found from experimental testing. By flowing water through the system with and without the nozzle attached and measuring the time for the change in volume at 1liter increments, the volume flow rate of the system, $\dot{V}$, can be measured. The volume flow rate can then be used to calculate the coolant average velocity, V_{avg}, and mass flow rate, $\dot{m}$ with Eqs. 1 and 2 when the density of the coolant, ρ, and the exit area, A, are known. Without the nozzle, the exit area is the inner diameter of the tubing, and with the nozzle, the exit area is the coolant exit area on the nozzle.

$$V_{avg} = \frac{\dot{V}}{A} \tag{1}$$

$$\dot{m} = \dot{V}\rho \tag{2}$$

Through the use of Bernoulli's equation, the dynamic pressure, P, at the exit of the coolant system can be calculated with Eq. 3 for a coolant with a known density and velocity.

$$P = \frac{1}{2}\rho V_{avg}^2 \tag{3}$$

When those calculations are performed without a nozzle, the resulting values provide the boundary conditions at the inlet of the nozzle for the computational model. When performed with a nozzle, the calculations provide the exit conditions, which can be used to validate the results of the computational model.

B. Previous Work

1. *Heat Transfer*

A. Ulas and E. Boysan[5] investigated the effects of the geometry and number of cooling channels, shown schematically in Fig. 2, in regeneratively cooled double-walled liquid propellant rocket engines, as well as the pressure drop across those cooling channels through finite element analysis and experimentation. They recreated an earlier experiment performed by Wadel and Mayer, and mathematically analyzed other devised scenarios in order to get an idea of general trends.[7] According to their model, the ideal number of channels for their LOX (liquid oxygen)/Kerosene fueled liquid rocket was 150. They discovered that increasing the number of cooling channels and increasing the aspect ratio improved the heat transfer and decrease the pressure drop, but only up to an optimum point. After, these effects are seen to decrease or even have overall detrimental effects on either pressure drop or heat transfer respectively. This current study will reproduce their model and apply it to our scenario, then compare the results to recorded data.

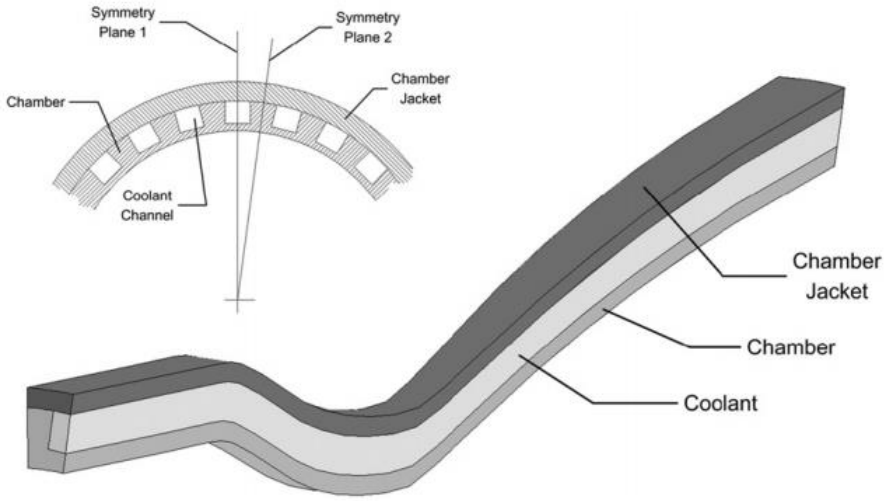

Figure 2: Regenerative cooling channels studied by Ulyas and E. Boysan[6]

Naraghi and Foulon[8] used basic fluid mechanics and heat transfer equations to study liquid hydrogen coolant properties throughout the Space Shuttle Main Engine (SSME). Their model functions independent of CFD (computational fluid dynamics) and is intended for rapid coolant property estimates where liquid hydrogen was injected at the nozzle exit and circulated towards the injector face. For the SSME, the calculated coolant pressure and temperature diverged from the more accurate RTE-TDK method. The inaccuracy displays a conditional use where it may be best utilized throughout the diverging section of the nozzle, up to the throat. This model is also limited by liquid hydrogen as the coolant; however, it is clear that the nozzle throat experiences the greatest heat flux, and the necessity for cooling is most vital at this area.

2. *Additive Manufacturing*

Carlile and Quentmeyer[9] studied cooling passage geometry for the outer wall of a liquid engine that was approximately 3 inches in diameter. Cooling passages were patterned radially, and liquid hydrogen flowed up the length of the engine. Fig. 3 shows an example of the simple, rectangular cooling passages like those used by Carlile and Quentmeyer. Three configurations were tested, each with thinner and more numerous cooling passages than the last. The small-scale liquid engine was fired hundreds of times noting temperature profile radially outward and number of cycles until failure. The baseline cooling passage configuration experienced engine failure after 200 cycles, and the engine with the thinnest cooling passages experienced no failure. Also, the thinnest cooling passage configuration resulted in a 30% decrease in wall temperature compared to the baseline configuration at the same pressure drop through the passages. The authors noted that the decreased wall temperature was expected because of increased cooling passage surface area. Therefore, the current study will evaluate the effectiveness of more cooling surface area due to the versatility of additive manufacturing.

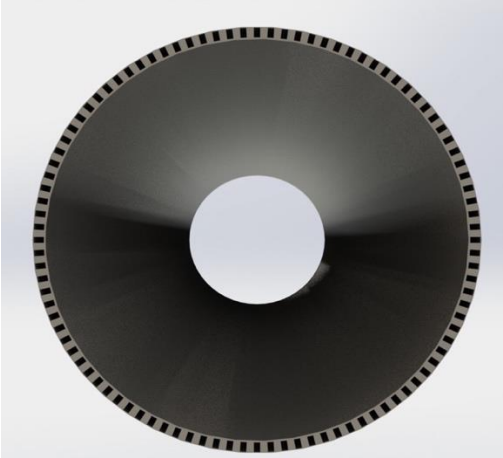

Figure 3: Example of Rectangular Cooling Passages Viewed from Downstream of a Nozzle

Kunka and Jacob[10] evaluated the capabilities and limits of additive manufacturing using Finite Deposition Modeling (FDM) and Stereolithography (SLA) in solid rocket nozzles. FDM is able to print with materials such as ABS (acrylonitrile butadiene styrene) or PLA (polylactic acid) while SLA uses a liquid polymer resin. Kunka and Jacob used a cold gas system to test nozzles at high pressures without exposing them to thermal effects. The cold gas testing showed that FDM is more susceptible to cracking at stress concentrations because of the layered printing method. Thermal testing with both regeneratively cooled and an ablatively cooled SLA nozzles showed higher than expected heat tolerance and some were able to be reused. For these reasons, the current study will use SLA for plastic prints and also note similar considerations for metal printing of different materials.

Fessl et al.[11] used additive manufacturing (AM) to print the liquid rocket engine they had designed. They used an EOS M290 metal printer that uses Selective Laser Sintering (SLS) to print with materials such as Inconel 718. They discuss how AM can save time, effort, and material but they also discuss some of the disadvantages of AM. With AM, part design is affected by the bed size, resolution, laser speed, laser power, heat transfer from bed to part, leftover powder inside the part, minimum thickness, orientation, shrinkage and overhang angles. For example, minimum part thickness must be larger than the printer's resolution. Additionally, when printing at an angle less than 45 degrees from the print direction, a support structure is needed to keep the part from collapsing. Fig. 4 shows the effects of greater overhang angle without support structure. The current study examines internal geometries where support structure may not be able to be removed and therefore will take these limitations into account during part design and limit internal geometries to a maximum of 30 degrees.

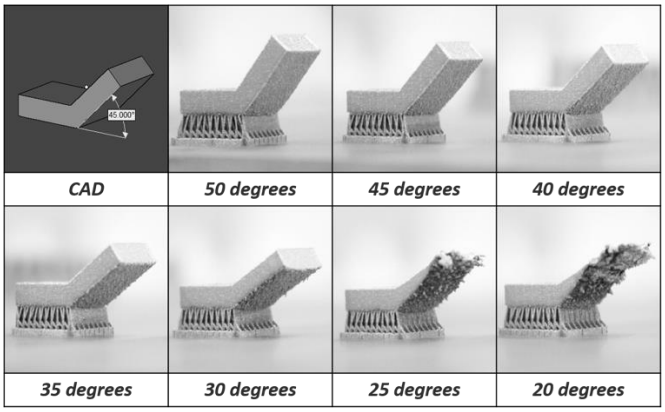

Figure 4: Example of Overhang Angle[12]

Herzog et al.[13] used literature published by many different authors to study the properties of additively manufactured metals and compare the static, tensile and fatigue limits to those of wrought or cast counterparts. They did not perform any experimentation, so they relied on other authors' data and information to reach a conclusion. Herzog et al. examined two aluminum alloys (AlSi12 and AlSi10Mg) with results from a cast sample and multiple

additively manufactured samples. The additively manufactured AlSi12 alloy displayed an average increase of 37% in yield strength, 9% in ultimate tensile strength, and 700% in elongation at failure over the cast material. The additively manufactured AiSi10Mg alloy displayed an average increase of 49% in yield strength, 33% in ultimate tensile strength, and 428% in elongation at failure over the cast material. These results show that additive manufacturing of metals can produce parts with a similar (if not better) structural capacity to those manufactured using traditional methods, but they elongate more before failure. The current study makes use of the results from these findings to provide an estimated structural capacity for the additively manufactured aluminum nozzle. Results are expected to differ because the current study will be working with more complex geometries and significant temperature increases.

III. Methodology

Sizing of the nozzle stemmed from a 1.5-inch outer diameter motor casing. This allowed 1.38 inches inside the casing for the nozzle. The nozzle throat and exit areas were sized based upon the Rocket Motor Components 29/38mm Nozzle, 0.291" throat. That nozzle is used in many 1.5" commercial rocket motors manufactured by Aerotech Consumer Aerospace.

A. Design

A 3" long propellant grain was modeled (Fig. 5) in the MotorSim software program, and for a chamber pressure of 500psi, the following nozzle dimensions were obtained: 0.2" throat and 0.5" nozzle exit.

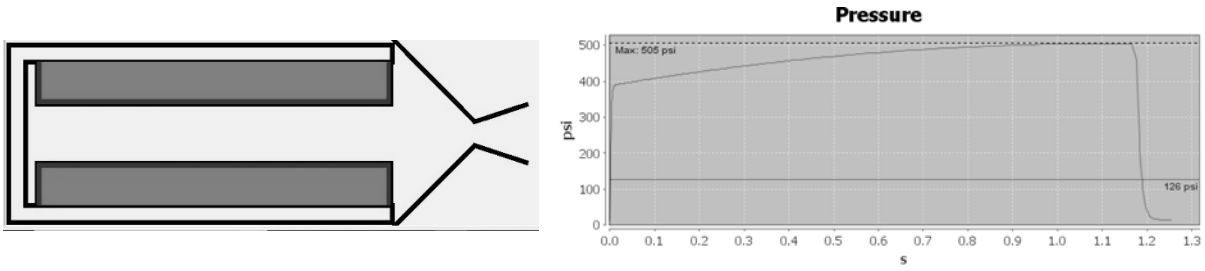

Figure 5. MotorSim Pressure Result for a 1 Grain KNSB Motor

For an overall nozzle length of 1.25" to fit inside a 1.38" ID aluminum motor casing with a forward closure and the propellant, the remaining nozzle dimensions were extrapolated. This resulted in an expansion ratio of 2.5. Optimization of the nozzle geometry for maximum efficiency is beyond the scope of this study. The final assembly for the rocket motor is shown in Fig. 6.

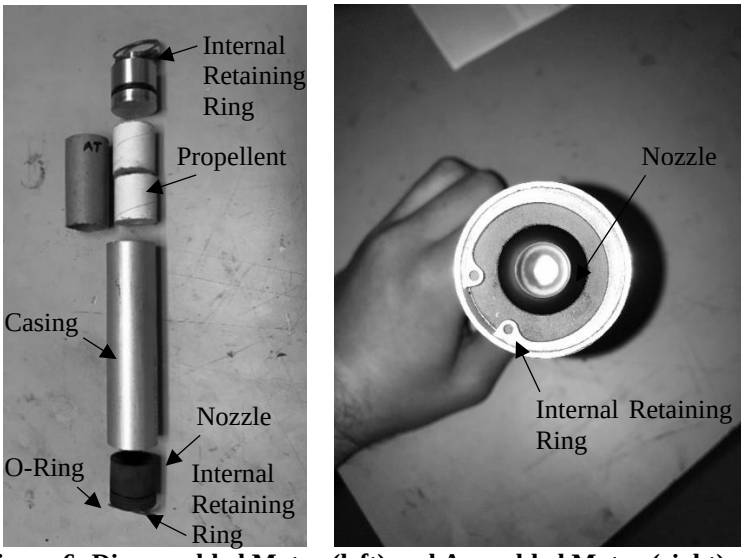

Figure 6: Disassembled Motor (left) and Assembled Motor (right)

Figure 7 (left) shows the nozzle design in Solidworks with the addition of several features. Figure 7 (right) shows a cross section of the design with hot gas flow traveling from right to left. The final design of coolant flow area features an inlet on the aft end of the nozzle. This inlet is exposed in a fully assembled motor, fitting between the gap in a 1-3/8" ID retaining ring.

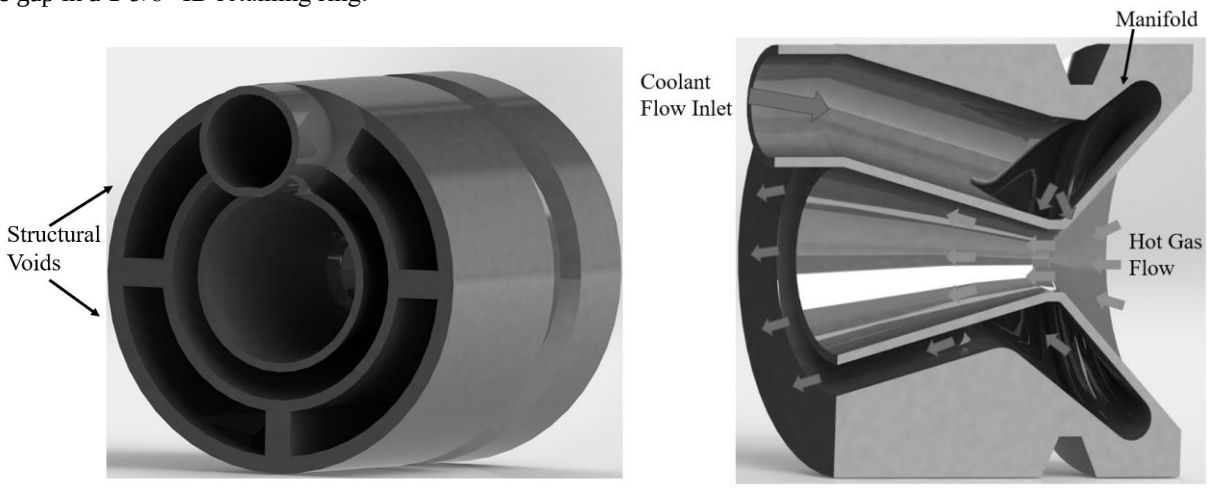

Figure 7: Solidworks Model of Nozzle Design (left) and Flow Schematic (right)

The feed system tube is attached and sealed with a friction fit around the inlet. After entering the inlet, the nozzle geometry feeds the coolant down the length of the nozzle, and the coolant is emptied into the manifold at the forward end of the nozzle. After filling the manifold, the coolant flow is forced to turn and travel the length of the nozzle again. The coolant then exits the nozzle on the aft end through which it entered. The full-annulus of flow provides for coolant contact over the entire surface area of the hot gas outer wall.

Figure 7 (left) shows an isometric view of the full part. This view also shows the O-Ring groove near the forward end of the nozzle which is used to seal the hot gas inside the motor case. Also visible in Figure 7 (left) are structural voids that reduce the part volume and print time by 26%.

The final nozzle design resulted from the need for even distribution through the coolant flow area, so that the coolant contacts the entire hot gas outer wall. The design was iterated with several plastic, 3-D printed prototypes, cold flow testing and gradual adjustments in coolant geometry. Cold flow testing descriptions are outlined in Section III.C.

B. Cold Flow Experimental Setup

Fig. 8 shows an overall picture of the overall cold flow testing setup. The experiment was conducted by inserting one end of the 0.4in x 3ft tube into the supply reservoir. The tube was run through the wood platform along the front support so the coolant would be able to flow vertically down from the supply reservoir. For the computational model boundary condition calculations, the coolant was run without an attached nozzle. For the computational model comparison values, the tube was attached to the nozzle coolant inlet. A vise clamp was used to clamp the hose to keep the water from running out between test. The testing started with the supply reservoir being filled with over 15 liters of water. The vise clamp was released to allow the flow of water, and the time was recorded at each liter mark starting at the 15-liter mark until the water level reached 3 liters. The volume flow rate, average velocity, and average exit pressure for each interval were then calculated. Stopping the measurement at 3 liters allowed for minimal transient effects.

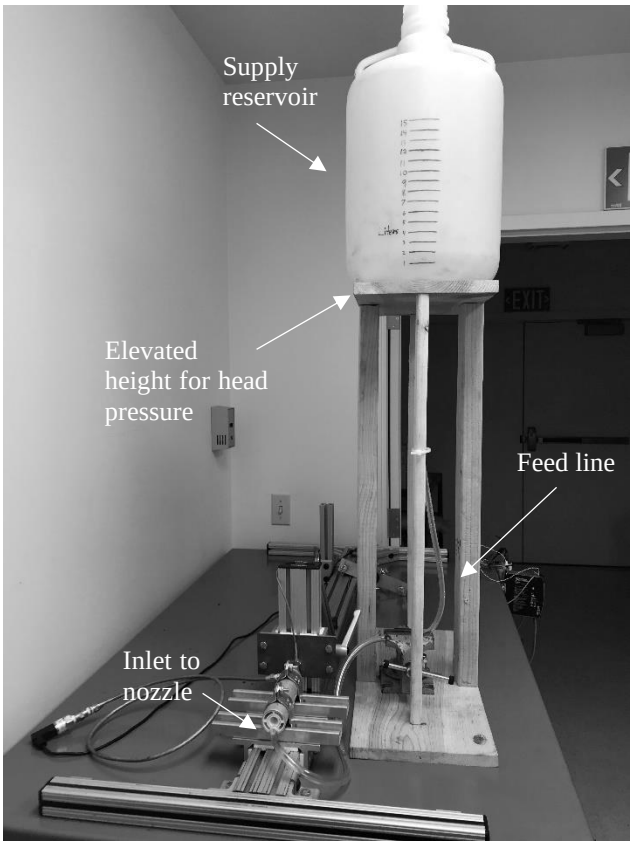

Figure 8: Coolant Feed System Integrated with Thrust Stand

While trying to find a nozzle configuration that would provide sufficient coolant flow to the entire nozzle wall, a design matrix was formed to compare nozzle coolant performance. Table 1 shows parameters such as throat diameter, inlet orientation, manifold size, tube size, and coolant area thickness were changed to maximize the nozzle cooling flow. Along with timing the coolant flow rate, a visual inspection was performed to determine if the nozzle would produce a full annular flow as seen in Fig. 9.

Figure 9. Full Volume Flow

Table 1: Design Matrix for Nozzle

Mark	Throat Diameter	Side Inlet	Bottom Inlet	Smaller Manifold	Exit Restrictions	Bigger Feed Tube	Coolant Area Thickness
1	0.18"	X					0.05"
2	0.455"		X				0.1"
3	0.455"	X		X			0.1"
4	0.455"		X	X		X	0.1"
5	0.455"		X	X		X	0.05"
6	0.455"		X	X		X	0.065"
7	0.2"		X			X	0.065"
8	0.2"		X			X	0.085"
9	0.2"		X	X		X	0.085"
10	0.2"		X	X	X	X	Variant
11	0.2"		X			X	0.1"

Data collected during the cold flow testing procedure was entered into a MathCad file designed to calculate the volume flow rate, mass flow rate and average flow velocity at the nozzle exit using Eqs. 1 and 2. Because a successful nozzle requires the coolant flow to fill the entire volume of the internal cavity, any nozzle design that did not pass the visual inspection for volume filling was not considered viable. Results were extrapolated from the comparisons between the nozzle iterations, and the validity of the computational model was examined against the experimental results.

C. Hotfire Experimental Setup

All hotfire motor tests were done on a portable thrust stand designed and built for evaluating solid rocket motor performance located at the Oklahoma State University Richmond Hill Research Center. Rocket motor and nozzle assembly test articles are prepared at the stand itself, located outdoors at the Richmond Hill north loading dock which faces away from the building, roads, and personnel. The water feed system is assembled first, with the rocket motor stored away to minimize the possibility of water contacting the propellant grains. 3 feet of elevation provides the necessary pump head for proper coolant operation as shown in Fig. 7. The feed lines are adjusted near the rocket motor for installation. With the feed system in place, the thrust stand is pushed against a concrete wall of the Richmond Hill north loading dock, and wheels are locked in place to limit movement during test preparation and motor firing. The pre-assembled rocket motor is secured to the stand at this time. The flat forward face of the motor is pushed flush against the stand's load cell for thrust measurements, and the motor secured by means of routing clamps on the stand's linear bearings as seen in Fig. 10 below.

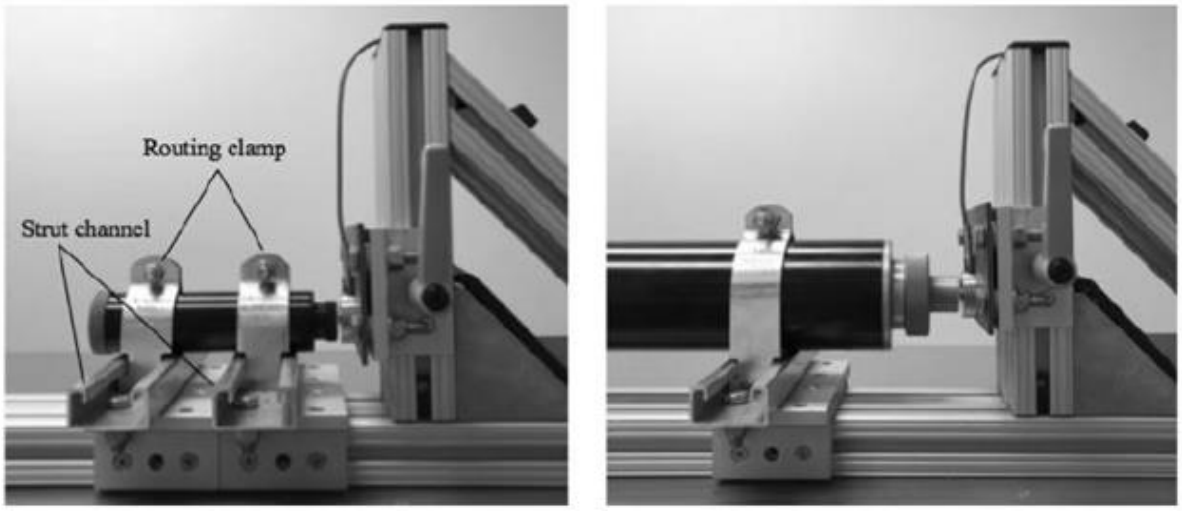

Figure 10: Thrust Stand Setup with Load Cell, Bearings, and Translations[14]

A 3D-printed plug as shown in Fig. 11 is inserted into the diverging nozzle section to help prevent any leaking water from entering the motor combustion chamber. An e-match used for the motor ignition is run through the plug to the motor. The feed hoses are then attached to the nozzle.

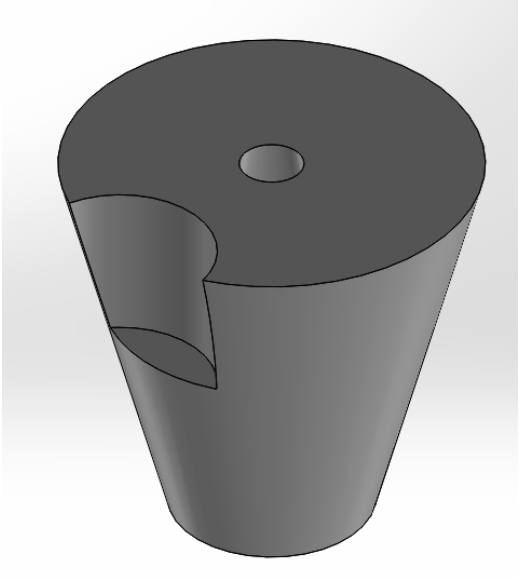

Figure 11. Nozzle Plug

When the stand has been prepared for the test article and the motor igniter is installed, the feed system is activated by loosening the vice clamp. Once the water is flowing properly, the area is cleared of personnel, and electrical power is supplied to the stand for ignition and data acquisition purposes. The 15-liter reservoir provides enough water for 4 minutes of flow through the nozzle, so should there be any complications with motor ignition, the stand, or anything else, the water need not be immediately refilled.

The rocket motor is ignited via the stand's LabView Virtual Instrument (VI) and thrust and pressure measurements are collected at this time. This VI is shown in Fig. 12 below.

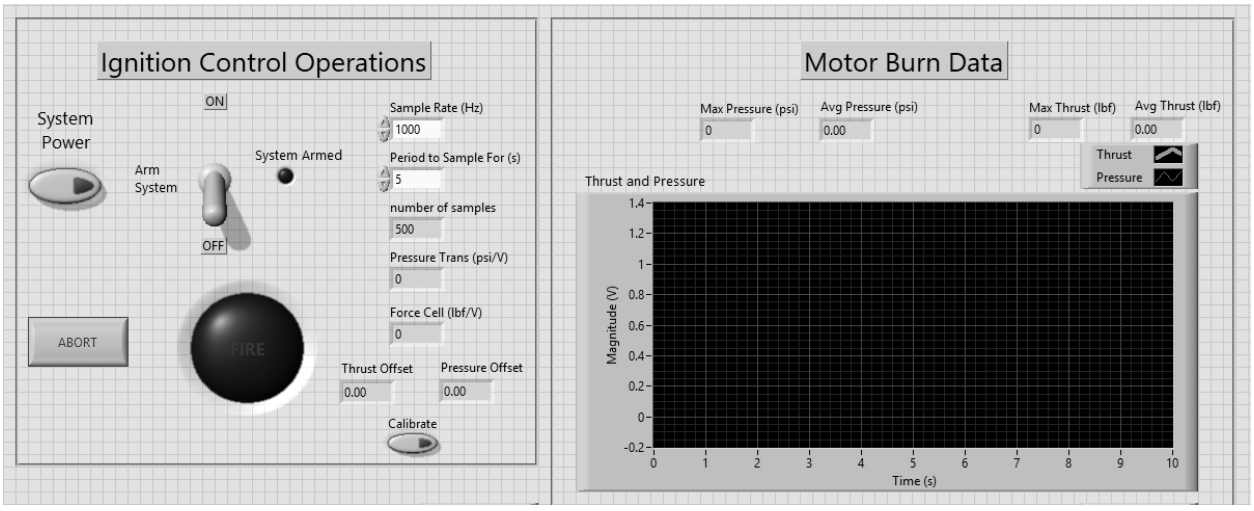

Figure 12: Thrust Stand Control VI and DAQ

Once the motor has completed its burn, the stand is approached, and the water feed line clamped. The motor is allowed to cool completely before releasing from the thrust stand and post-test evaluations are performed on the nozzle including visual inspection, dimensions taken, and mass measurements of the nozzle part individually.

IV. Results

A. Cold Flow Data

For any iteration to be considered, it has to fill the coolant passage volume. This was a visual test to confirm the water was flowing out of the entire exit from the coolant passage. Fig. 13 shows a Mark 8 nozzle on the left that did not pass the test due to the water only coming out of the bottom, while a Mark 11 nozzle on the right did pass the test. If the nozzle iteration did not pass the volume fill test, measurements were not conducted for flow rates because this was a necessary condition for the nozzle to perform successfully.

Figure 13: Mark 8 Nozzle Left (Unsuccessful Exit Flow) and Mark 11 Nozzle Right (Successful)

Table 1 shows how changing geometric parameters resulted in an evenly distributed coolant flow. The throat diameter was increased from 0.18” to 0.455” between Marks 1 and 2 so the nozzle would fit snugly into the commercial rocket casing. Due to Mark 2 not having an evenly distributed coolant flow, Marks 3 through 6 were designed with a 45 % smaller manifold so the amount of water used would completely fill the manifold. Mark 3 was undesirable because it used a side inlet, which required a hole to be drilled into the side of the rocket casing, affecting future reuse. Marks 4 through 6 provided the full annular flow needed to fill the coolant passage volume. It was found that decreasing the coolant area thickness (shown in Fig. 14) between Mark 4 and Mark 5 helped evenly distribute the flow. Due to leftover residue from the printing operation, from Mark 5 to Mark 6, the coolant area thickness was increased, so the residual printing material could be removed. From Mark 6 to 7 the throat diameter was then decreased from 0.455” to 0.2” to scale the nozzle to fit the research rocket casing, but Mark 7 did not produce the same annulus of flow. Increasing the coolant area thickness from Mark 7 to 8 did not have enough effect on the increasing the flow area, so the manifold size was decreased for Mark 9. The flow was moving at a high velocity out of the nozzle opposite the coolant inlet, but the exit area near the inlet was not receiving any coolant flow. In an attempt to divert flow, an obstruction was implemented into the design for Mark 10. The coolant still did not cover the entire exit area, so the coolant area thickness and manifold size were increased above the original Mark 7 value for Mark 11, and the nozzle exit achieved a full annulus of flow. This nozzle design as seen in Fig. 14, was the only research rocket nozzle that passed the volume fill test. Due to time constraints, there were no more iterations beyond the Mark 11, which was used for hotfire testing in both low infill and high infill prints.

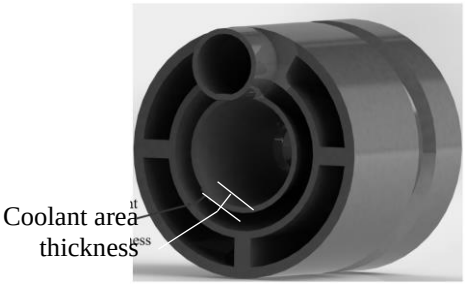

Figure 14: Example of Coolant Area Thickness

After performing the procedures described in Section III.B., the average coolant system exit velocity was found to be 5.01 ft/s and the total exit pressure was found to be 14.87 psi. These values were then used as the boundary conditions for the computational model. Because Mark 11 was the only successful iteration of the research rocket motor nozzles, it was the focus of the computational model validation. The procedure from Section III.B. was used with the nozzle, and the nozzle exit velocity was found to be 28.2 ft/s and the total exit pressure was found to be 20.06 psi. These values will be compared with the values from the computational model in Section IV.C.

B. Hotfire Data

8 different configurations of motor firings are shown in Table 2. PLA was the primary print material due to its accessibility, and the infill density was studied to determine if additional internal structure mass had an effect on nozzle performance. Two geometries were printed: an uncooled variant that consisted of the converging and diverging profile, but no coolant passages; and second, the same converging diverging profile, but with integrated coolant geometry distribution and feed design. The latter was also test fired without coolant flowing, as to study the effect of the cooled nozzle geometry alone during the motor firing. A photo of a cooled PLA nozzle in operation is shown in Fig. 15. Part of the coolant feed system is also visible: the clear hose, the vice to restrict the flow between tests, and the wood support structure that held the coolant reservoir above the thrust stand.

Table 2: Hotfire Nozzle Configuration Matrix

Nozzle Configuration #	Material	Infill Density	Uncooled/Cooled Geometry	Cooled geometry with Coolant
1	PLA	Low (15%)	Uncooled	
2	PLA	High (70%)	Uncooled	
3	PLA	Low (15%)	Cooled	
4	PLA	High (70%)	Cooled	
5	PLA	Low (15%)	Cooled	X
6	PLA	High (70%)	Cooled	X
7	SLS Nylon	N/A	Uncooled	
8	SLS Nylon	N/A	Cooled	X

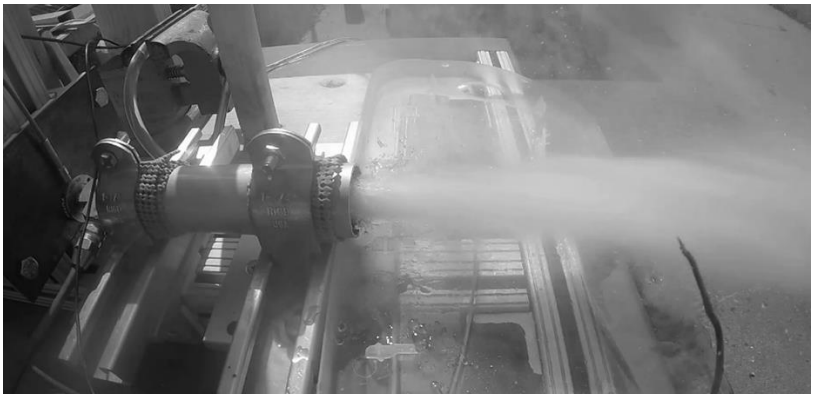

Figure 15. Cooled PLA Nozzle in Operation During Motor Burn

The parameter of greatest interest was nozzle throat diameter change due to ablation before and after the burn because throat diameter and area are fundamental to a nozzle's geometry. The greatest heat flux occurs at the nozzle throat[1]; therefore, the greatest ablation will also occur at the nozzle throat. According to Fig. 16 the uncooled PLA nozzles widened the most with an average throat area increase of 129%. A cooled, high-infill PLA nozzle had a 105% difference which was the least amount of ablation for all the PLA nozzles. This figure shows that higher infill prints with liquid cooling reduced throat ablation; however, the nozzles still suffered too much damage to be deemed a worthwhile nozzle or suitable for reuse. The SLS nylon also presents promise as an improved nozzle material over PLA, withstanding the heat and pressure with less ablation than PLA. However, the cooled SLS nylon featured similar changes in throat diameter to the PLA nozzles, indicating issues with the nozzle design itself rather than ineffective material choice.

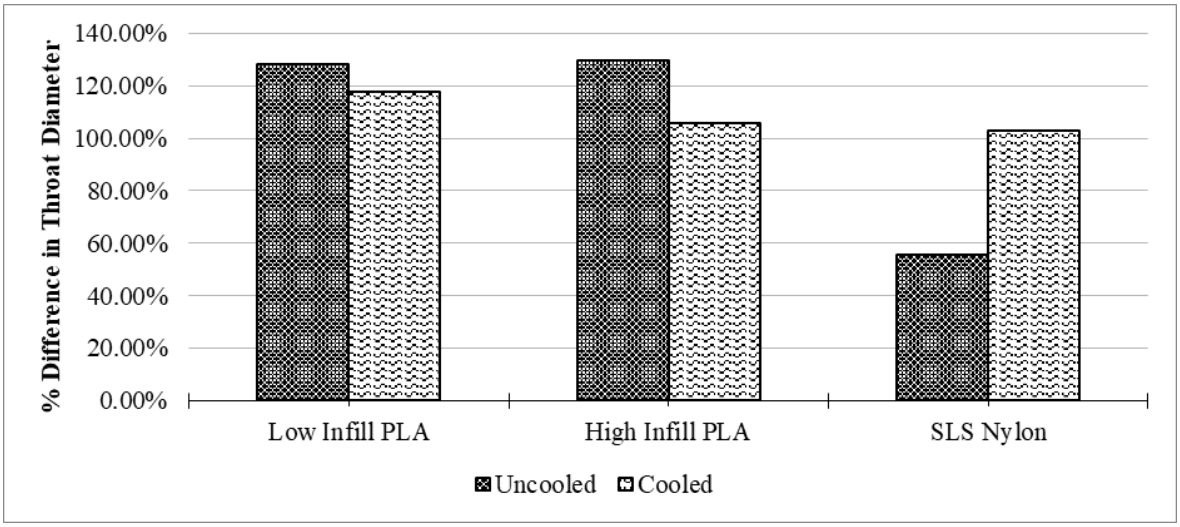

Figure 16. Nozzle Type and Percent Difference in Nozzle Diameter, Before and After Hotfire

For those same nozzles, the change in mass was also calculated as a result of the firing. The burned nozzles were often fragile, so care was taken during disassembly not to damage the nozzle further. Fig. 17 represents the mass data. Cooling favorably affected the nozzles by reducing the material ablation and mass loss compared to uncooled test articles. One consideration to note is that the radial mass distribution was not equal for the uncooled and cooled nozzle geometries. On the uncooled nozzles, more mass was concentrated and distributed near the throat and was therefore ablated away with the widening throat area. This could explain the greater percentage of the uncooled nozzle's mass loss.

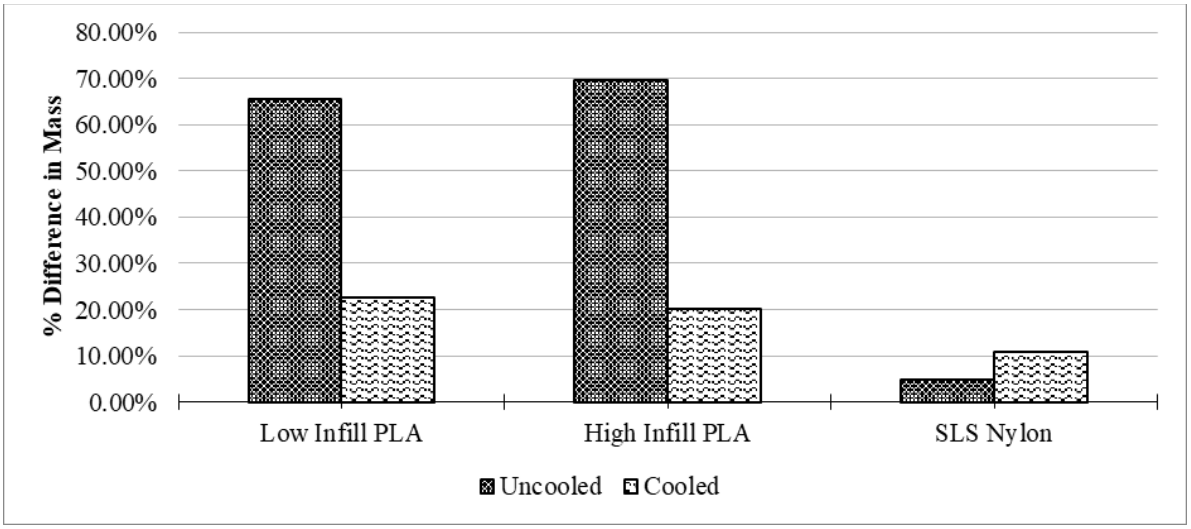

Figure 17. Percent Difference in Mass from Before and After Motor Firing

The SLS nylon was an improved material choice to PLA. Fig. 18 shows data for the uncooled configurations where SLS nylon is compared to the low and high infill PLA nozzles.

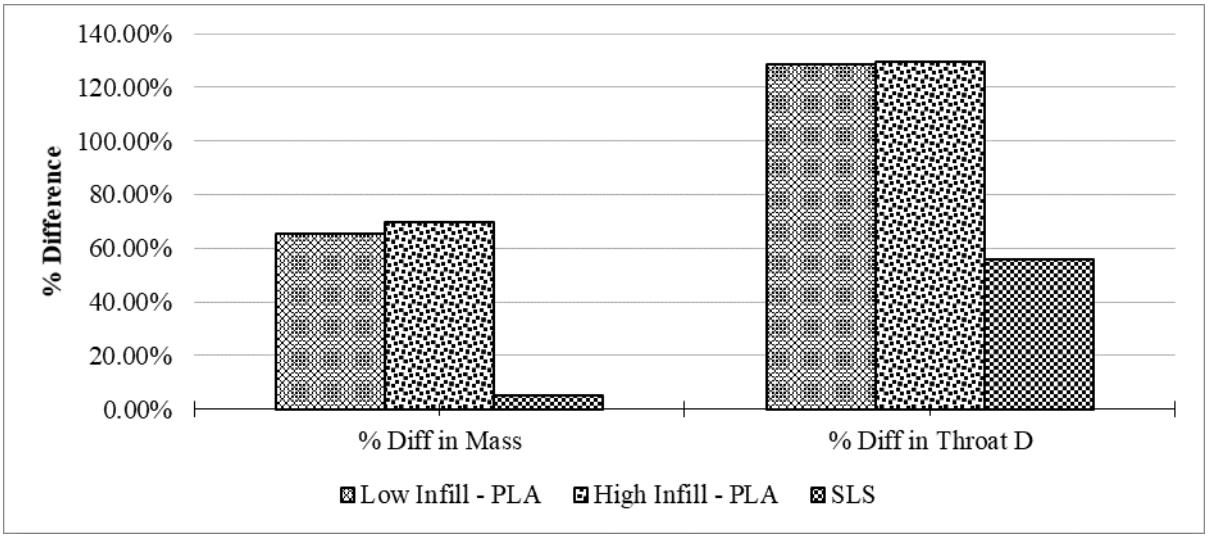

Figure 18. Uncooled Nozzle Material Type and Percent Difference in Mass and Throat Diameter

The PLA nozzles lost significant mass, differing by as much as 69% from the starting mass. The SLS however, only lost 1.1g, or 5% of its mass. Throat diameter ablation was also reduced by the SLS, with a 56% difference in mass versus over 120% for both the low and high infill PLA nozzles. The uncooled SLS nozzle outperformed the PLA and is a superior material for rocket nozzle applications.

By visual inspection, none of these nozzles were suitable for reuse. Each suffered significant damage, regardless of cooling effects. On each, the throat area was widened, mass lost, and coolant geometry damaged altogether. A collective photo comparison is shown Fig. 19.

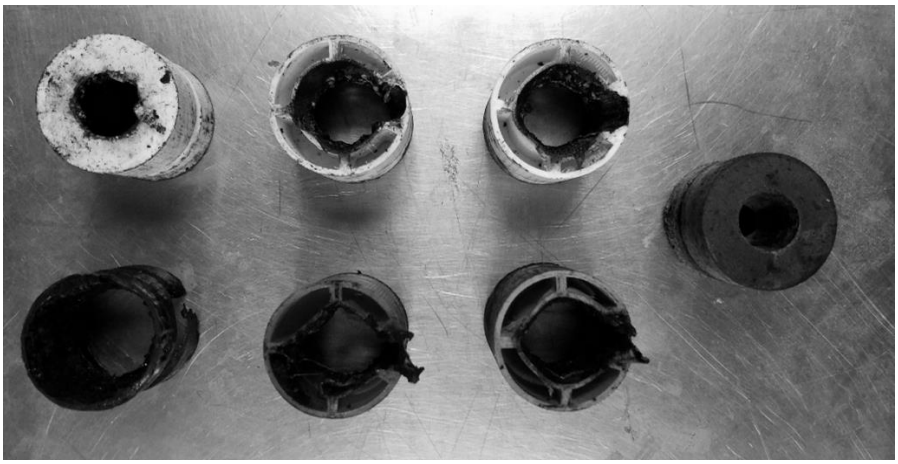

Figure 19. From Top Left Going Clockwise: Nozzle Configuration 2, 4, 6, 7, 5, 3, 1 Post-Firing (See Table 2)

In addition to the data presented on the nozzles themselves, thrust and pressure data was also collected during these motor burns. As the SLS nylon uncooled nozzles maintained their geometry best, losing minimal mass and a comparatively small increase in throat diameter, it produced the highest thrust and pressures as shown in Fig. 20. Next to it is a thrust curve from a PLA nozzle with low infill and cooling. It does not achieve as high thrust or pressure with large fluctuations at 1.5s where the nozzle disintegrated and failed.

The associated motor grain is a cored cylinder and exhibits slightly progressive thrust and pressure behavior due to its geometry. However, as the SLS nozzle ablates and throat widens, the internal pressure drops, but thrust remains largely constant. Thus, an overall neutral burn profile was achieved as a result of the nozzle throat ablation.

This is seen also in plot to the left in Fig. 20. This same behavior is not observed in the right plot because of the damage to the nozzle.

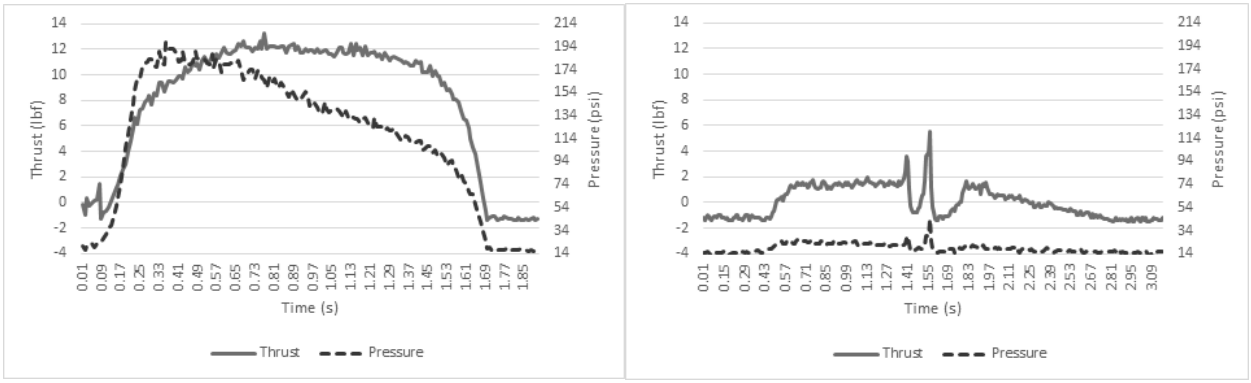

Figure 20. SLS Nozzle (left) and PLA Low-Infill Cooled Nozzle (right) Thrust Curves

Following inspection of video of many of these firings, the cooled nozzles tended to fail in a common way, regardless of the nozzle material. Within a second following motor ignition, the coolant feed hose would be blown off of the nozzle, ending the coolant flow through the nozzle's coolant passages. This was theorized to be due to initial throat widening that ablated into the coolant passages, increasing the backpressure on the coolant feed tube, thereby blowing it off. Without the water, the heat and widening throat geometry continued to ablate the remaining nozzle geometry. This observation suggests a nozzle redesign is in order to increase the nozzle wall thickness so that some minor ablation can occur before contacting the coolant passage walls. Furthermore, even the more heat-resistant SLS nylon exhibited the same behavior as the PLA, indicating the ablation may be due to internal pressure and mass flux, rather than just temperature causing thermal material deformation.

C. Thermal and Fluid Modeling

Damage to the inner side of the hot gas wall caused by ablation is related to the temperature distribution inside the wall. Temperature distribution in the hot gas wall is examined analytically in the current study due to difficulties in experimental measurement. The temperature distribution can be estimated using Computational Flow Dynamics (CFD) and Finite Element Analysis (FEA) using ANSYS Fluent software and the knowledge of hot gas and coolant temperatures at the boundaries. Experimental results from cold flow testing, and known grain burning temperatures were used to provide the necessary boundary conditions for the model. As the flow conditions are not fully developed within the nozzle, due to the low characteristic length of the flow path and ever-changing geometry, the flow can be considered as a transitional or a mixing flow. Thus, it is necessary to compare several models of flow in order to determine the best description. However, given that the fluid is water, which has a relatively low viscosity, it will be more like turbulent flow than laminar. Two such turbulence models have been selected for comparison: K-Epsilon (Fig. 21) and K-Omega (Fig. 22). Therefore, boundary conditions were as shown in Table 3. Both inlets were velocity inlets, and the outlets were both to constant atmospheric pressure, which is the value given as exit pressure. Materials were modeled as PLA for the solid, water as the coolant, and water vapor as the hot gas.

Table 3: Model Boundary Conditions

Nozzle Location	Pressure (Pa)	Thermal (K)	Type
Hot Gas Inlet	200000	700	Velocity Inlet
Hot Gas Outlet	1020	270	Pressure Outlet
Cooling Inlet	1052530	270	Pressure Inlet
Cooling Outlet	1020	270	Pressure Outlet

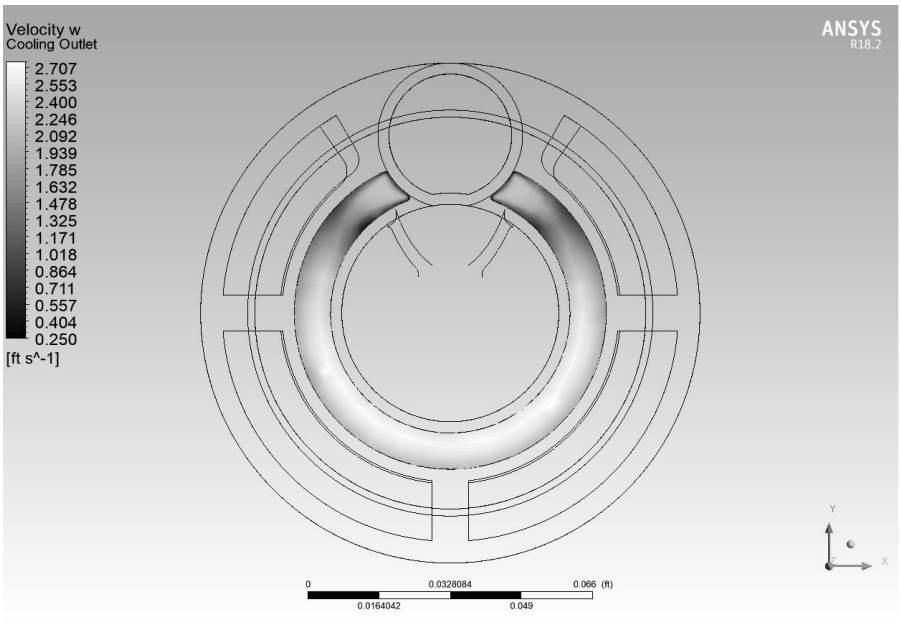

Figure 21: K-Epsilon Model Velocity Profile

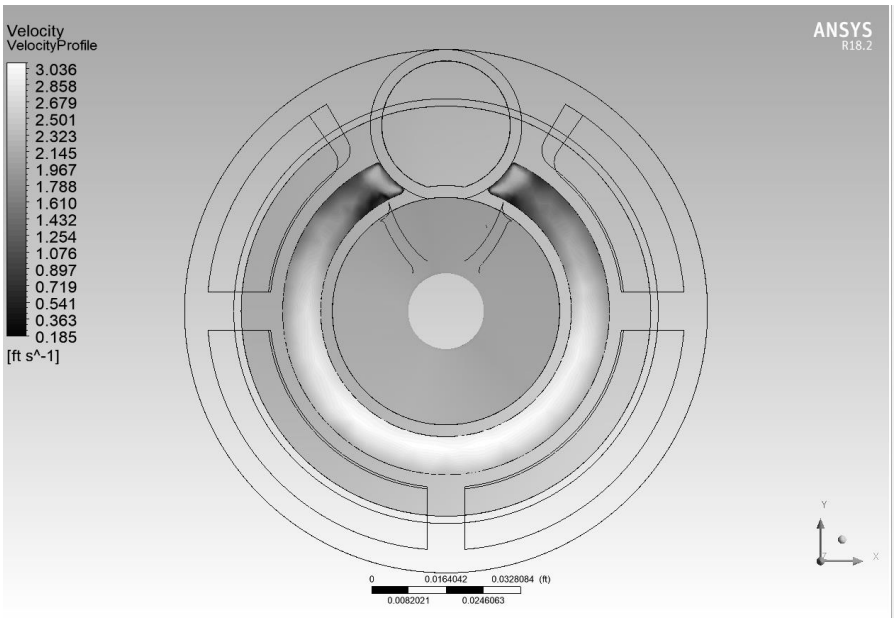

Figure 22: K-Omega Model Velocity Profile

The resultant velocity was significantly different from velocities observed in cold flow testing. However, the resultant mass flow was markedly similar. For the cold flow testing mass flow was .077 kg/s, which was significantly similar to both the K-Omega model, and the K-Epsilon model. Between .077 kg/s from cold flow testing and .088 kg/s for the CFD model, there is only an 8.5% difference. As expected, the K-Omega model overpredicts the turbulence, such that the resultant velocity is much less than the cold flow modeled velocity.

This model provides a framework for future design of the rocket nozzles, surface ablation can be greatly reduced if the temperature distribution across the interior wall is reduced. Temperatures shown are likely in good agreement with temperatures shown in experiments. As seen in Figure 23, the inside wall temperature is significantly greater than the melting temperature of the PLA, it is unsurprising that it failed. Theoretically, the combination of heat and thrust was enough to eject or melt and compress the center of the geometry that surrounded the cooling flow.

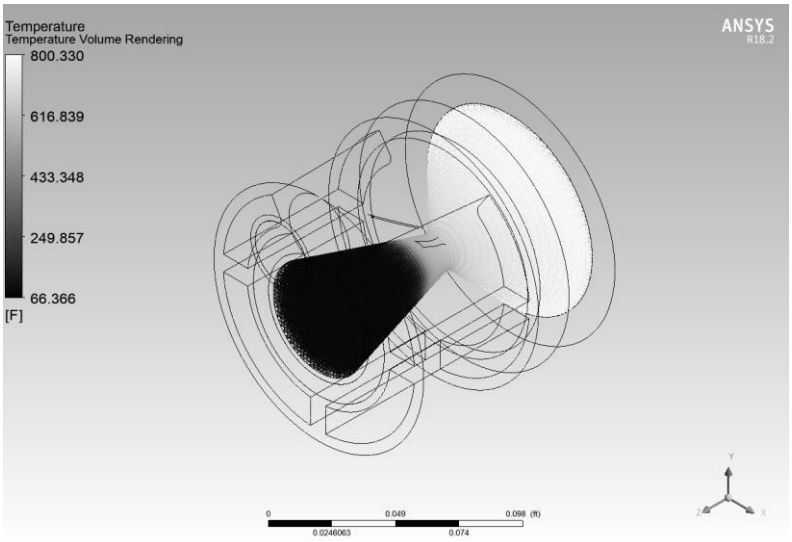

Figure 23: K-Epsilon Temperature Volume Rendering of Hot Gas

Sources of error in the model include assumptions, mathematical errors and measurement errors. Instead of a boundary condition that assumed zero velocity and only an inlet temperature, it might have been more accurate to have assumed that the entire volume of the combustion zone was a consistent temperature or that inlet velocity was higher. This would improve the accuracy of the thermal aspect of the model. Computational error can be assessed via the residual graphs and final residual values. As far as the model is concerned, one such source of error is the mesh. A high-quality mesh would have a minimum of ten elements across the smallest characteristic geometry of the model thus allowing a smooth curve over the profile. The current model has a minimum of five. A third type of error is that of a round under error, in which, significant digits of the intermediate values are lost from the calculation at some or all steps. It seems that there is some built-in protection for this within ANSYS, as early calculations returned error messages until the mesh refinement was increased. However, double-bit precision calculations would provide some extra protection from this as well.

V. Conclusions and Recommendations

The additively-manufactured, liquid-cooled nozzle presented in this paper demonstrates the potential and feasibility for small-scale rocket propulsion hardware to not only be 3D printed, but also integrate internal cooling passages. While PLA and SLS nylon, uncooled or cooled, are not directly suitable for rocket nozzles in this configuration and application, the effects of cooling are discernable and could be even more effective with more resilient materials than such polymers. The results only covered these two materials, but other printed materials such as aluminum and steel offer potential for nozzle applications. A cooled nozzle redesign with thicker nozzle and coolant walls may improve resistance to ablation as well. Other data should be collected, primarily temperature throughout the nozzle and measuring the coolant temperature increase as a result of flow through the nozzle to help validate CFD and other analytical data.

Future testing should include more firings with each nozzle, multiple firings on a single nozzle, and longer rocket motor burns with greater mass and heat flux through the nozzle.

Acknowledgements

The authors would like to thank Thomas Coulon and Garrett Wilkens for their assistance in propellant manufacture and test firing. They would also like to thank Dr. Kurt Rouser for materials and advisement.

References

[1] Sutton, G.P., Biblarz, O., *Rocket Propulsion Elements*, 7th ed., John Wiley & Sons, Inc., Hoboken, NJ, 2010, pp. 288.

[2] Sutton, G.P., Biblarz, O., *Rocket Propulsion Elements*, 7th ed., John Wiley & Sons, Inc., Hoboken, NJ, 2010, pp. 288.

[3] Sutton, G.P., Biblarz, O., *Rocket Propulsion Elements*, 7th ed., John Wiley & Sons, Inc., Hoboken, NJ, 2010, pp. 286.

[4] Sutton, G.P., Biblarz, O., *Rocket Propulsion Elements*, 7th ed., John Wiley & Sons, Inc., Hoboken, NJ, 2010, pp. 306.

[5] A. Ulas, E. Boysan, Numerical analysis of regenerative cooling in liquid propellant rocket engines, Aerospace Science and Technology, Volume 24, Issue 1, 2013, Pages 187-197, ISSN 1270-9638, https://doi.org/10.1016/j.ast.2011.11.006.

[6] A. Ulas, E. Boysan, Numerical analysis of regenerative cooling in liquid propellant rocket engines, Aerospace Science and Technology, Volume 24, Issue 1, 2013, Page 188, ISSN 1270-9638, https://doi.org/10.1016/j.ast.2011.11.006.

[7] Mary Wadel and Michael Meyer NASA, Lewis Research Center, Cleveland, OH NASA, Lewis Research Center, Cleveland, OH 32nd Joint Propulsion Conference and Exhibit Published : July 1, 1996 Online Date : February 19, 2013 DOI : 10.2514/6.1996-2584

[8] Naraghi, Mohammad & Foulon, Matthieu. (2008). A Simple Approach for Thermal Analysis of Regenerative Cooling of Rocket Engines. ASME International Mechanical Engineering Congress and Exposition, Proceedings. 10. 10.1115/IMECE2008-67988.

[9] Carlile, J., Quentmeyer, R., & Lewis Research Center. (1992). An Experimental investigation of high-aspect-ratio cooling passages (NASA technical memorandum ; 105679). Cleveland, Ohio : [Springfield, Va.: National Aeronautics and Space Administration, Lewis Research Center ; For sale by the National Technical Information Service.

[10] Kunka, L., Jacob, J.D. "Evaluation of Low Cost Additive Manufacturing Techniques for Small Rocket Nozzles", 58th AIAA/ASCE/AHS/ASC Structures, Structural Dynamics, and Materials Conference, AIAA SciTech Forum, (AIAA 2017-1829).

[11] Fessla, J. (2018). Liquid Rocket Engine Design for Additive Manufacturing Jan Fessla*, Hanmo Shenb, Nihar Patelb, Tai Wei Chena, Suyash Ghirnikarb, Martin Van Den Berghec.

[12] Utley, Eric. "An Introduction to Designing for Metal 3D Printing." The SOLIDWORKS Blog, 29 June 2017, blogs.solidworks.com/solidworksblog/2017/06/introduction-designing-metal-3d-printing.html.

[13] Herzog, D., Seyda, V., Wycisk, E., Emmelmann, C., "Additive Manufacturing of Metals," Acta Materialia, Vol. 117, 2016, pp. 371-392.

[14] Foster, G.C., Utley, L.J. "Design and Test of a Portable, Flexible-Use Rocket Thrust Stand", 2019 AIAA Student Paper Competition, Region IV.

[15] Sutton, G.P., Biblarz, O., *Rocket Propulsion Elements*, 7th ed., John Wiley & Sons, Inc., Hoboken, NJ, 2010, pp. 287.